ISSN 1392 - 1207. MECHANIKA. 2014 Volume 20(1): 49-56

Numerical prediction of NO_x emissions in a full-scale furnace

A. Mokhtardidouche*, A. Benarous, L. Loukarfi***, H. Naji******

*Hassiba Benbouali University, B.O. 151, Chlef, 02000, Algeria, E-mail: mokhtardidouche@gmail.com

**Hassiba Benbouali University, B.O. 151, Chlef, 02000, Algeria, E-mail: a.benarous@univ-chlef.dz

***Hassiba Benbouali University, B.O. 151, Chlef, 02000, Algeria, E-mail: l.loukarfi@yahoo.fr

****Artois University & University of Lille, Northern France, Laboratoire Génie Civil et géo-Environnement (EA 4515), Technoparc Futura, F-62400 Béthune, France, E-mail: hassane.naji@univ-artois.fr

crossref http://dx.doi.org/10.5755/j01.mech.20.1.3904

Nomenclature

A_p - product constant; A_R - reactant constant; c_p - specific heat, kJ/kg/K; C_μ - turbulence model constant; D_b - *b*urner diameter, m; D_{ch} - furnace diameter, m; D - diffusion coefficient, m^2/s; h - sensible enthalpy, kJ/kg; $\tilde{k}$ - turbulent kinetic energy, m^2/s^2; $k+$ - forward rate constant, $kmol/m^3/s$; $k-$ - reverse rate constant, $kmol/m^3/s$; L_{ch} - furnace length, m; M_i - molecular weight, kg/kmol; N - total number of chemical species; p - static pressure, Pa; Pr_T - *t*urbulent Prandtl number; r - radial coordinate, m; R_i - rate of formation, $kg/m^3/s$; $R_{i,j}$ - reaction rate, $kmol/m^3/s$; S - swirl number; S_h, S_R - volumetric heat sources, $kJ/m^4/s$; T - temperature, K; U: Axial velocity, m/s; u - velocity vector, m/s; $u^{"}$ - fluctuating velocity vector, m/s; W - tangential velocity, m/s; x, X - *a*xial coordinate, m; Y_i - *m*ass fraction; $\tilde{\varepsilon}$ - dissipation rate, m^2/s^3; μ_t - turbulent viscosity, kg/m/s; ρ - density, kg/m^3.

1. Introduction

Nowadays, national and international current legislations incite industrialists to optimize their processes to strongly reduce pollutants emissions. This is particularly true for cement production units, where substantial quantities of nitrogen oxides (NO_x) and carbon dioxides (CO_2) are produced due to high temperatures required for clinkering [1]. In spite of all the efforts realized during the twenty last years, the emission of such kind of primary pollutants is always very important. With regard to this issue, nitrogen oxide plays an important role in main of actual environmental problems. Because about 60% of the global emissions of the hazardous pollutants are believed to come from combustion processes [2], it can be envisaged to reduce significantly this way of production. The first way consists in a better and direct control of the combustion process to limit the production of the primary pollutants. In this context, air or fuel combustion staging can be used to reduce NO_x emissions but the performance is limited because a high temperature zone is required to sinter the clinker. The increase of carbon monoxide (CO) levels as the result of using Low NO_x Burners (LNBs) is also unfavorable to the necessary oxidation of the clinker components, whether it occurs in the high-temperature sintering or lower-temperature calcinations sections [3]. There have been some successes in using low primary air burners for rotary kilns, in which the non-premixed flame is diluted by hot products [4].

A secondary way consists in the use of an appropriate treatment of the gaseous effluents before rejection to the atmosphere. In this category, we can cite the NO_x reburning technique, the selective catalytic reduction (SCR), the selective non catalytic reduction (SNCR) and the advanced gas reburning (AGR) [5, 6]. While Urea and Ammonia-based SNCR seems well suited for cement kilns in terms of NO_x reduction, its implementation costs are substantially higher than those associated with the primary methods, by as much as a factor of 10 [7].

From a theoretical context, the problems of flow and heat transfer in industrial furnaces and combustors are of a complex nature, and hence attention must be focused on the general principles which govern the behavior of the flow in such configurations [8]. According to this, the mathematical model of processes in the combustion chamber consists of four basic segments: turbulent flow, convective heat and mass transfer, chemical reactions and radiative heat transfer.

Because of device costs, experimental techniques in full-scale furnaces are mainly limited to localized measurements. Moreover, due to tremendous heat fluxes, data acquisition from flame neighboring is not obvious even with a use of non-intrusive techniques [9]. In addition, in-situ predictive analyses require kiln operations at various injection flow rates for which production break-off is often necessary. Consequently, numerical combustion modeling of such practical systems needs precise and quality predictions. Here, the computational fluid dynamics (CFD) represents a reliable tool for predicting emissions levels while allowing for low-cost design solutions.

The main aim of this work is to test the ability of a CFD analysis to recover the flow field pattern as well as NO emissions for a full-scale cement kiln. Reynolds averaged numerical simulations (RANS) are performed in both non-reactive and reactive cases. The mathematical formulation of the standard $k-\varepsilon$ turbulence model is slightly modified to account for round jet effects and numerically implemented within the solver. An attempt towards NO depression by using a swirling configuration of the primary air is also presented.

This paper is organized to including the following sections: flow, chemistry and radiation modeling, computational domain, and boundary conditions are introduced in Section 2. Section 3 presents and comments selected numerical simulation results in terms of temperature and velocities profiles, streamlines for various swirl numbers, and NO thermal contours. Finally, some conclusions drawn from this study are made in Section 3.

2. Fluid dynamic computation

2.1. Problem Set-up

The configuration considered here is that of a full-scale kiln designed for cement production and implemented to carry out this study. The burner is equipped with a shear-coaxial element linked to a cylindrical chamber with an internal diameter $D_{ch} = 5$ m and a length $L_{ch} = 100$ m. The burner is made of a central conduct ($D_b = 0.25$ m) for the fuel surrounded by 75 mm wide annulus for the primary air. The annular space (2.3 m) between the burner and the chamber body is used for flue gases injection which is considered as a co-flow stream. Axisymmetric model for the furnace is adopted for the calculations. It is composed of three velocity inlets, a circumferential wall and an outlet with a prescribed static pressure (Fig. 1).

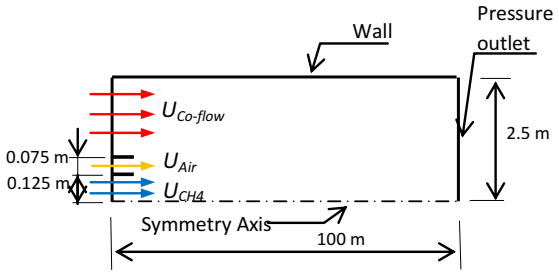

Fig. 1 Schematic diagram the computational domain

2.2. Turbulent flow modeling

The time-Favre averaged (Density weighted time averaging) form for each extensive quantity (except pressure and density) is considered leading to the Favre averaged Navier-Stokes equations, which can be expressed as the following:

continuity:

$$\frac{\partial \bar{\rho}}{\partial t} + \frac{\partial \bar{\rho}\tilde{u}_i}{\partial x_i} = 0\,; \tag{1}$$

momentum:

$$\frac{\partial \bar{\rho}\tilde{u}_i}{\partial t} + \frac{\partial \bar{\rho}\,\tilde{u}_j\tilde{u}_i}{\partial x_j} = -\frac{\partial}{\partial x_j}\left(\bar{p}\delta_{ij}\right) + \frac{\partial}{\partial x_j}\left(\bar{\tau}_{ij} - \overline{\rho\, u_i^{''}u_j^{''}}\right); \tag{2}$$

energy:

$$\frac{\partial\left(\bar{\rho}\,\tilde{h}\right)}{\partial t} + \frac{\partial\left(\bar{\rho}\,\tilde{u}_j\tilde{h}\right)}{\partial x_j} = \\ = \frac{\partial}{\partial x_j}\left(\overline{\rho D\frac{\partial h}{\partial x_j}} - \overline{\rho\, u_j^{''}h^{''}}\right) + \frac{\partial \bar{p}}{\partial t} + S_h + S_R\,, \tag{3}$$

where $\bar{\tau}_{kj}$ are the viscous stress component, $\overline{\rho\, u_k^{''}u_j^{''}}$ are the so-called Reynolds shear stress, $\overline{\rho\, u_k^{''}h^{''}}$ are the turbulent heat fluxes, S_h, S_R refer to rates of heat release and loss due respectively to combustion and radiation processes, and h denotes the sensible enthalpy of the mixture given by:

$$\tilde{h} = \sum_{\alpha} Y_\alpha\left(\Delta h^0_{F,\alpha} + \int_{T_0}^{T} c_{p_\alpha}(T)\,dT\right), \tag{4}$$

where Y_α, $\Delta h^0_{F,\alpha}$ are respectively the mass fraction and formation enthalpy of the species α. In the previous set of equations, body forces have been neglected.

Note that turbulent shear stress and turbulent heat fluxes are modeled to achieve closure via viscosity and diffusivity assumptions as follows:

$$\overline{\rho\, u_i^{''}u_j^{''}} = -\mu_T\left(\frac{\partial \tilde{u}_i}{\partial x_j} + \frac{\partial \tilde{u}_j}{\partial x_i} - \frac{2}{3}\frac{\partial \tilde{u}_k}{\partial x_k}\delta_{ij}\right) + \frac{2}{3}\bar{\rho}\tilde{k}\delta_{ij}\,; \tag{5}$$

$$-\overline{\rho\, u_j^{''}h^{''}} = \frac{\mu_T}{Pr_T}\frac{\partial \tilde{h}}{\partial x_j}\,, \tag{6}$$

where $Pr_T = 0.7$ is the turbulent Prandtl number, and μ_T is the turbulent viscosity, given by:

$$\mu_T = C_\mu \bar{\rho}\,\tilde{k}^2/\tilde{\varepsilon}\,, \tag{7}$$

where C_μ is a constant, $\tilde{k}\left(=\overline{u_i^{''}u_j^{''}}/2\right)$ is the turbulent kinetic energy and $\tilde{\varepsilon}$ is its the dissipation rate.

Note that the Reynolds stress term $\overline{\rho\, u_k^{''}u_j^{''}}$ is defined in the literature both as shown here, as well as with the opposite sign, and sometimes without the density included in the definition. This different terminology does not matter, as long as consistency is maintained throughout the derivation.

The previous system is completed by model transport equations for the turbulent kinetic energy $\tilde{k}$ and its dissipation rate $\tilde{\varepsilon}$ [10]. It should be noted that the model transport equation for $\tilde{k}$ is derived from the exact equation, while the model transport equation for $\tilde{\varepsilon}$ can be obtained using physical reasoning and bears little resemblance to its mathematically exact counterpart.

2.3. Chemical reaction modeling

The analysis requires a suitable scheme for coupling the turbulent mixing and the reactions of major species. In this paper, oxidation of methane can be defined by the use of the general two-step reaction mechanism [11]:

$$CH_4 + \frac{3}{2}O_2 \longrightarrow CO + 2H_2O\,; \tag{8}$$

$$CO + \frac{1}{2}O_2 \longrightarrow CO_2\,. \tag{9}$$

The effect of combustion on flow is estimated using the source terms of the species transport equation and the energy equation. The rate of production or consumption R_i of the ith species is determined by considering the contribution of each reaction:

$$R_i = M_i\sum_{j=1}^{2} R_{ij}\,. \tag{10}$$

As we deal with a non-premixed turbulent flame, one uses an algebraic model with a linear relaxation expression for the reaction rates. The turbulent mixing is

adopted to be the controlling step in the reaction rate definition. According to the works of Magnussen and Hjertager [12], the large-eddy mixing time-scale, defined as $\tilde{k}/\tilde{\varepsilon}$ governs the chemical reaction rate. The dissipation rate of turbulent eddies R_{ij}^{R} and R_{ij}^{P} for reactants (R) and products (P), are introduced:

$$R_{ij}^{R} = -\upsilon_{i,j}\rho A_{R,j}\frac{\varepsilon}{k} min\left(Y_R / \upsilon_{R,j} M_R\right); \quad (11)$$

$$R_{ij}^{P} = \upsilon_{i,j}\rho A_{P,j}\frac{\varepsilon}{k}\frac{\sum_{P} Y_P}{\sum_{m=1}^{N}\upsilon_{m,j} M_m}, \quad (12)$$

where A_R and A_P are empirical constants for each reactive flow. The governing rate is then expressed by $R_{ij} = min\left(R_{ij}^{R}, R_{ij}^{P}\right)$.

2.4. Radiation modeling

In order to correctly predict the temperature distribution in the furnace a radiative transfer equation (RTE) for an absorbing, emitting and scattering medium was solved. Once the radiative intensity is obtained, the gradient of the radiative heat flux vector was found and substituted into the enthalpy equation to account for heat sources (or sinks) due to radiation. The solution of the RTE for this application was obtained using the discrete ordinates (DO) radiation model [13].

2.5. NO_x emission modeling

As it was stated by Hill et al. [14], the rates of formation of nitrogen oxides (NO_x) are slower than those of the most combustion products (CO_2, H_2O, CO, O_2, CH_4). The production of such pollutant species only marginally affect the combustion process and do not influence the flame characteristics. Decoupling NO_x prediction from flame calculations is therefore a common practice in the simulation of combustion systems. In most of the combustion cases NO accounts for about 95% of the total NO_x [15]. Nitrogen oxides (NO_2) and nitrous oxide (N_2O) are less significant components of the total NO_x formation. Therefore one only accounts for NO species, for which the formation rate can be attributed to the following kinetic processes.

2.5.1. Thermal NO_x mechanism

Thermal NO_x is formed by the oxidation of atmospheric nitrogen at high temperatures. Although the Zeldovitch mechanism has been introduced as early as 1947, it continues to be widely used in both theoretical and application studies [15]. In the present paper, the Zeldovitch mechanism of thermal NO is adopted for NO formation.

The NO_x formation is significant only at high temperatures because fixation of nitrogen requires the breaking of the strong N_2 triple bond (dissociation energy of 941 KJ mol^{-1}) [14]. When there is sufficient oxygen, as in a fuel lean flame, the overall rate of consumption of free nitrogen atoms becomes equal to the rate of its formation and therefore quasi-steady states can be established. Hence the NO formation rate becomes:

$$\frac{d[NO]}{dt} = \frac{2[O]\left(k_{+1}k_{+2}[O_2][N_2] - k_{-1}k_{-2}[NO]^2\right)}{k_{+2}[O_2] + k_{-1}[NO]}. \quad (13)$$

It should be noted that with this assumption, the only quantity left undetermined is [O] since O_2 and N_2 concentrations are predicted from the combustion solution.

2.5.2. Oxygen atom model

The kinetics of the thermal NO_x formation rate is much slower than the main hydrocarbon oxidation rate, and most of the thermal NO_x is formed after completion of combustion. The assumption of equilibrium can be justified by a reduction in the importance of radical overshoot at higher flame temperature [16]. Partial equilibrium is an improvement to equilibrium; it is achieved by accounting for third-body reaction in the O_2 dissociation-recombination process:

$$O_2 + M \rightleftarrows O + O + M. \quad (14)$$

In this situation, the O radical reaction rate is achieved as follows:

$$[O] = 36.64\times10^{5} T^{0.5}[O_2]^{0.5} exp\left(-27123/T\right). \quad (15)$$

2.6. Numerical investigations

Favre averaged Navier-Stokes equations are considered for the incompressible flow within the furnace. The system is completed with the transport equations for $\tilde{k}$ and $\tilde{\varepsilon}$ as well as species mass fractions. The operating scheme is based on a prediction of the velocity field followed by a pressure correction step. Equations for turbulence and scalars are solved separately afterward. The space discretization is based on the fully conservative structured finite-volume framework with a fully collocated arrangement for all variables. The steady state computations have been performed using the commercial CFD-Ansys-Fluent solver [17].

2.7. Boundary conditions

It is known from early investigations on full-scale furnaces [18] and also our numerical experience that boundary conditions values strongly influence the quality of the predictive calculations. According to measurements over a period of thirty days [19], time averaged values for fuel, primary air and co-flow velocities were believed to be constant. To ensure a dilution of the reaction zone, a portion of the flue gases is mechanically driven within cylindrical conducts into the furnace entrance. The corresponding inlet velocity for the co-flow is 0.265 m/s. Moreover, the exhaust fan mounted at the exit section of the furnace yields a slight depression $\Delta p_{in-out} \approx -300$ Pa. Boundary conditions for turbulence are set by specifying the hydraulic diameter and turbulent intensity. This quantity was adjusted in a fashion to recover the measured NO level at the furnace exit.

Numerical values for boundary conditions are reported in Table.

Table

Boundary conditions specification

	Fuel	Primary air	Co-flow	Side Wall of the furnace	Furnace exit section
Type of boundary condition	Velocity Inlet	Velocity Inlet	Velocity Inlet	Wall	Pressure outlet $p_{out} = 101000$
Temperature, K	283.15	298.15	1300	Adiabatic	------
Velocity, m/s	72.44	330.0	0.265	-----	------
Hydraulic diameter, m	0.25	0.15	4.60	------	5.00
Turbulence intensity, %	10	10	5	------	-------

3. Results and discussion

The numerical simulation was carried out on an axisymmetric domain. A non-uniform unstructured mesh composed of 39.000 cells was used. To determine the appropriate grid with computational efficiency, series of computational tests with finer grids (up to 70.000 cells) show that the quality of the prediction was not improved by enhancing the number of cells (Fig. 2). So, we opted for the first mesh since it seems a best trade-off between the accuracy and the computation time.

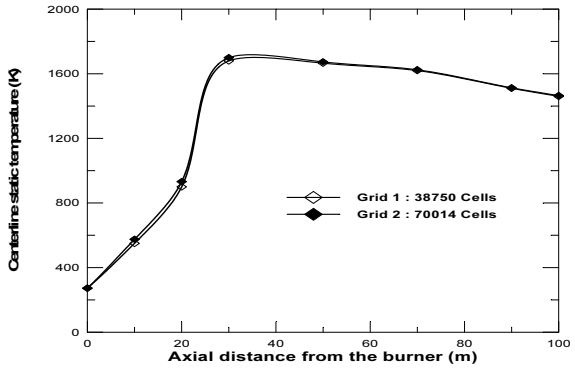

Fig. 2 Mesh sensitivity study based on the centerline temperature

As the reactants are diluted with hot products, the oxygen rate in the flues gases will eventually influence the flame characteristics. In this context, a thermochemical analysis [20] was performed on the methane-air equilibrium combustion under atmospheric conditions. The study shows the influence of the oxygen dilution rate on the adiabatic flame temperature (AFT) as well as on the stoichiometric ratio (Fig. 3).

The case of 9% O_2 is particularly important since it corresponds to measurements data [19]. In this situation, an important decrease of 43% is noticed on the adiabatic flame temperature (AFT) when oxygen dilution ranges from 21% which refers to fresh-air injection to 9%. Moreover, the stoichiometric point moves towards the high mixture ratio values which reveals a reduction in the fuel consumption for a specified heat release. Accordingly, flame dilution by combustion products restricted to flammability considerations, is believed to be a reliable technique for temperature reduction and hence for NO_x depression.

An efficient solution strategy in combustion problems consists in using a so-called "cold flow" simulation as a first step. Here the species transport equations are solved without considering the production source terms. It is particularly interesting because it separates the effect of turbulent mixing from combustion such that one can validate the

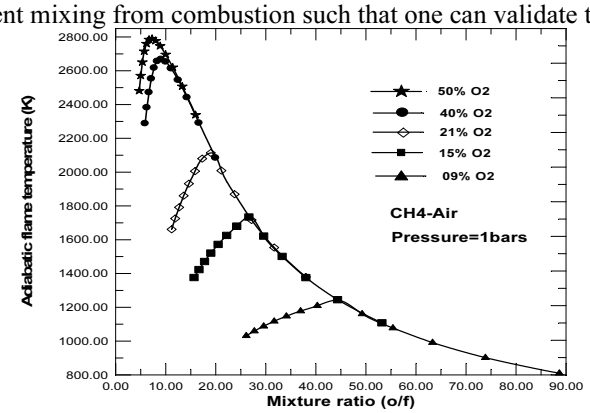

Fig. 3 Adiabatic flame temperature at different mixture ratios

appropriate turbulence model. Cold flow simulation can also provide a "good" guess solution field for reactive calculations.

A previous study [21] regarding the actual shearing injection case has shown that the standard $k-\varepsilon$ model allows for satisfactory prediction of the static pressure within the kiln. Particularly for the wall pressure coefficient which agrees quite well with the measurements. However, the size of the recirculation zone due to important velocity gradients between reactants streams and co-flow was considerably overestimated.

In the aim to enhance the prediction of the turbulent dynamic field, one should account for round jet effects within the furnace. As it was stated by Pope [22], one has to add an additional term in the ε transport equation. The major modification consists in tuning the $C_{2\varepsilon}$ constant of the standard $k-\varepsilon$ model, from its default value to $C_{2\varepsilon} = 1.84$. More details regarding the implementation of the Pope correction can be found in [22].

Fig. 4, a shows the distribution of the axial velocity at two radial locations $r = 1$ and $r = 2$ situated within the co-flow region. It is noticed that axial velocity at $r = 1$ m, shows a significant increase ($120\ \mathrm{m\,s^{-1}}$) over a 25 m distance downstream the entrance. This can be explained by a well prediction of the primary-air penetration into the co-flow region due to its radial spreading (round jet effects). Moreover, the co-flow region situated close to the wall ($r = 2$) reveals the existence of a reverse flow (negative axial velocity) in the axial range of 25 m to 55 m. The recirculation zone which is probably due to the strong shearing between the primary air and the co-flow, spreads axially over a 30 meter distance. In fact, neglecting the round effect of the jet leads to an underestimation of the radial penetration of the primary air. As a result, the axial

velocity is attenuated and the recirculation zone is overestimated by more than 73% (Fig. 4, b).

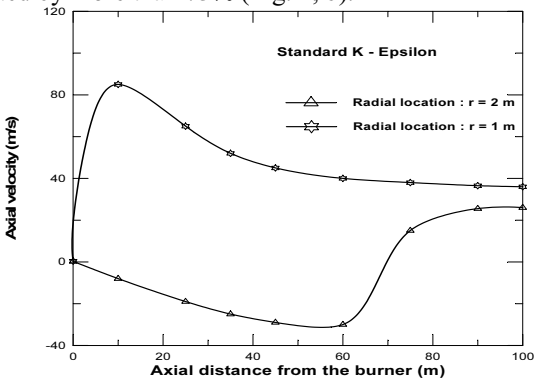

a

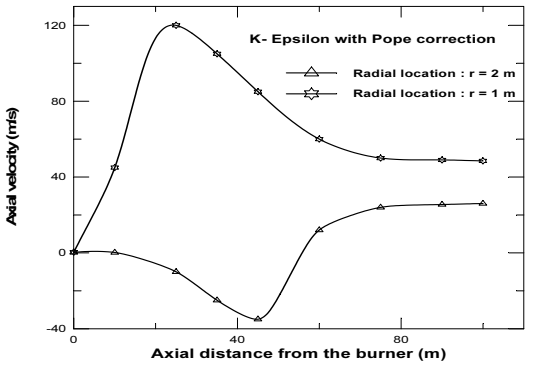

b

Fig. 4 Profile of X-velocity vs. the axial distance at two radial distances: a) standard $k-\varepsilon$ model; b) $k-\varepsilon$ with the Pope correction

Spatial distribution of the temperature as provided by the hot fire simulation depends strongly on turbulent mixing since the reaction rates are expressed in terms of large-eddies time scale ($\widetilde{k}/\widetilde{\varepsilon}$). Here, high temperature level locations occupy an important area (Fig. 5) from the top of the burner lips to the wall and extend axially on approximately 30 meters which is quite close to the size of the recirculation zone.

The non-premixed flame is therefore stabilized by the recirculation zone that acts as a "natural swirl" due to the dynamic field within the kiln. As observed in Fig. 5, the presence of a hot co-flow makes that the reaction zone shape does not correspond to a "standard jet" flame.

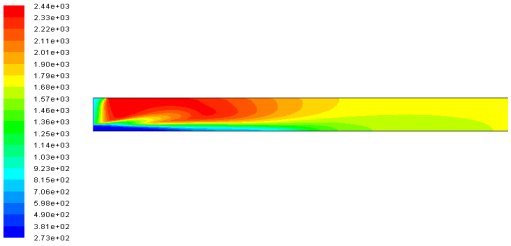

Fig. 5 Contour plots of the static temperature

At the exit section of the furnace, radial relaxation of the static temperature is noticed. The simulation overestimates by 8% the static temperature located on the centerline when comparing with the probe measurements [19] (Fig. 6). This discrepancy is certainly due to the simplifications introduced by the two-step mechanism which accounts only for three final products (CO, CO_2, H_2O). In addition, one always ignores H_2 formation and its impact on temperature profiles. As expected for full-scale simulations [9], flame calculation without accounting for radiation losses will result in a significant over-prediction of the thermal level. Here, the discrepancy in the static temperature reaches the threshold of 60% (Fig. 6).

Fig. 6 depicts the axial profiles of the static temperature at three radial locations, $r = 0$, $r = 0.125$ and $r = 2$. Across the furnace, the temperature profiles move from the highest values which refer to the co-flow region ($r = 2$) to the lowest ones that correspond to the centerline ($r = 0$).

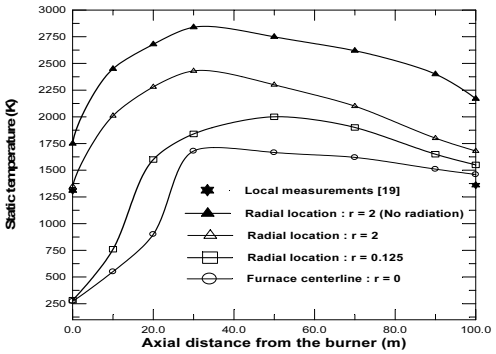

Fig. 6 Temperature distribution along the axial distance at various radial locations

Maximum carbon monoxide values (up to 1.92 ppm) are located in the mixing-layer zone separating fuel and the primary-air streams (Fig. 7). Indeed, the turbulent mixing which governs the rate of production of CO, is expected to be important in the mixing zone. Here, high values of turbulence intensity and velocity gradients may occur. These amounts of carbon monoxide are not recovered at the furnace exit. This behavior shows that the temperature relaxation at the exit section promotes the reverse reaction of CO transformation into CO_2.

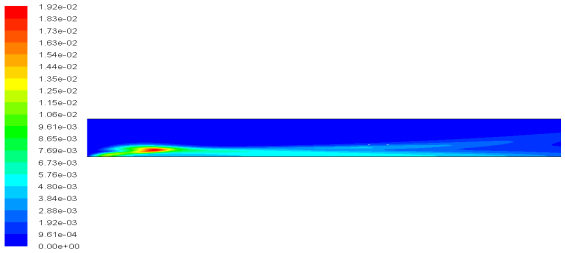

Fig. 7 Contour plots of the carbon monoxide

It is essential to remember that NO_x production is mainly influenced by stoichiometry (the availability of O_2) and temperature conditions (high temperature). Indeed, spatial contour of the thermal NO (Fig. 8, a) shows that a peak value of 3070 ppm is reached in a localized region which ranges from 35 to 65 m. However, this region is situated slightly downstream the recirculation zone where sufficient amounts of oxygen are encountered. Here, the lack of oxygen close to the co-flow zone is responsible for the decrease of the nitrogen oxide in spite of the high thermal level.

As it is the case for the static temperature, the NO level exhibits a radial quasi-uniformity at the furnace exit

section (Fig. 8, b). The averaged value of 1750 ppm is slightly greater than the point-measurement level (1600 ppm) of the centerline probe.

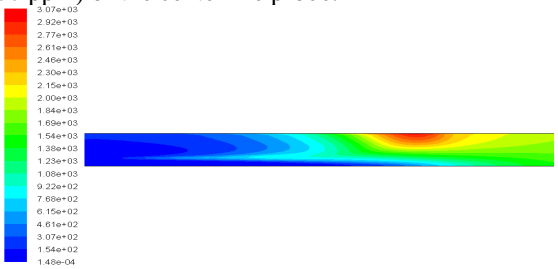

a

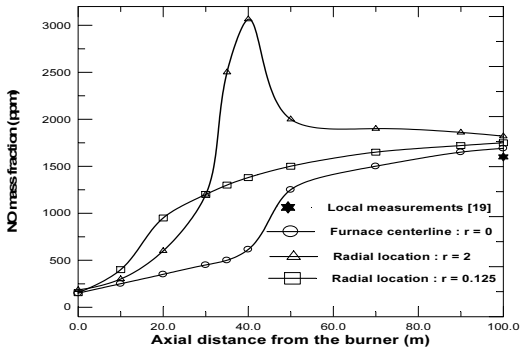

b

Fig. 8 a) Contour plots of the thermal *NO* mass fraction (ppm); b) *NO* mass fraction along the axial distance at various radial locations

It should also be stressed that from a technical point of view, the co-flow temperature at the furnace entrance may be lower than that of the flue gases at the exit section. Indeed, heat transfer between ducts and external environment may occur during the re-injection process, making questionable the adiabacity of the ducts. In this context, a numerical simulation was conducted for various co-flow temperatures in the aim of analyzing its impact on the exit *NO* level.

Fig. 9 shows the predicted *NO* distribution at the exit section at different co-flow temperatures. One notices that any decrease in co-flow temperature promotes a depression of the NO with a minimum threshold of 1550 ppm. Above the temperature value of 1330 K, the *NO* emission at the furnace exit section increases. The agreement between the numerical results and the measurements is quite acceptable, especially for high co-flow temperatures, where a relative deviation of 9.5% is noticed. However, high temperature values for the injected flue gases are not numerically significant since it exceed the AFT level (Fig. 3). Moreover, local measurements of such levels of temperature are certainly due to mixture ratio fluctuations and therefore, do not represent a stable operating point of the furnace [9]. It is also noticed that no measurements of *NO* are available below 1300 K. This is probably due to problems related to the clinker quality while operating in the range of moderate temperatures.

Regarding the possibility of *NO* depression, it is interesting to test numerically the implementation of one of the primary methods described previously. As it is known, combustion efficiency and stability are improved by good mixing between fuel and air as well as hot co-flows. Here, the splitting of the combustion air into coaxial and annular jets would therefore create an adequate vortex which enhances the mixing while allowing for NO_x depression [9].

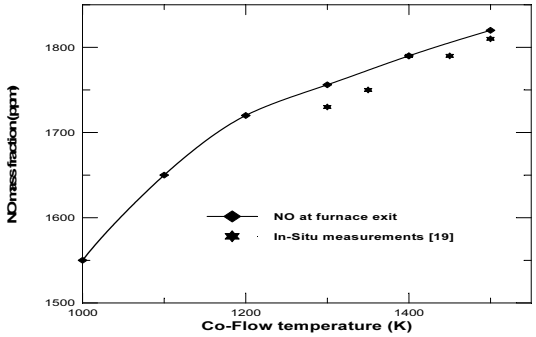

Fig. 9 *NO* distribution vs. co-flow temperatures at the exit section

Properties of the swirl flow can be correctly described by the swirl number according to the following formula:

$$S = 2G_\theta / DG_x, \tag{16}$$

where D is the stream diameter, G_θ is the tangential momentum flux and G_x is the axial momentum flux. This expression can be simplified to:

$$S = \int_0^R \rho UWr^2 dr \Big/ R\int_0^R \rho U^2 r dr, \tag{17}$$

where U and W are the axial and circumferential of the flow stream.

In the following, an attempt towards reducing the global *NO* emissions at the furnace exit section is proposed. For this purpose, one considers that the stream of the primary air is delivered by a swirler injector with a prescribed swirl number S_0. It should be noted that, when operating at various swirl number S_0, the mass flow rate of the fuel was adjusted in a manner to maintain the same value of the overall mixture ratio as for the original (shear) injection configuration.

It is well known that the standard $k-\varepsilon$ model is not suited to describe mixing within swirling flows [23]. The main reason is the aforementioned assumption of the isotropic behavior of the Reynolds stress tensor, which is generally not verified inside swirled flames, where each individual stress may develop differently. Hence, we use the Reynolds stress model (RSM) which closes the Reynolds-averaged Navier-Stokes equations by solving transport equations for the Reynolds stresses, together with an equation for the dissipation rate [24].

For practical consideration, it is desirable to have a high swirl to achieve adequate mixing and decrease residence time in hot swirling zones while limiting the production of NO. However, the associated strain rates must not be so large to make the flame close to the burner.

With regards to the jet dynamics within the furnace (Fig. 10), the use of a low or a moderate swirl causes an extension of the main recirculation zone in the axial direction. The low swirling values of the primary air ($S_0 \le 0.5$) seems to be in favor of an axial rather than a radial development of the recirculation zone. As the swirl

number increases, pattern of the stream functions is affected by the high strain between the primary air and the co-flow. The main recirculation zone shows an axial shrinking while trapping the flue gases in a corner region close to the burner (Fig. 10). On the other hand, static temperature profile along the axial distance within the mixing zone ($r = 0.125$), offers better clarification of the relation between the imposed swirl number S_0 and the flame-burner distance (Fig. 11). Indeed, axial position of the maximum static temperature moves from $X = 46$ meters which refers to the non-swirling case ($S_0 = 0$) to less than one meter for a strong swirl ($S_0 = 0.8$). In this situation the flame is almost attached to the burner head.

Moreover, the static temperature at the radial location $r = 0.125$ exhibits an asymptotic behavior revealing that the central recirculation zone (CRZ) prevents the hot co-flow to spread radially while yielding an important gradient of temperature. For an important swirl $S_0 = 0.8$, the relative depletion in static temperature at the exit section is about 14%. This can be explained as follows: Owing to the strong swirl, the flue gases are trapped in a corner recirculation zone (Fig. 10) and the thermal diffusion to the exit is therefore attenuated in favor of a global diminution of the static temperature, and thus, of the *NO* emission rate.

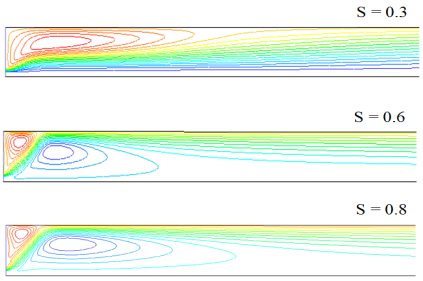

Fig. 10 Stream function contours for various swirl numbers

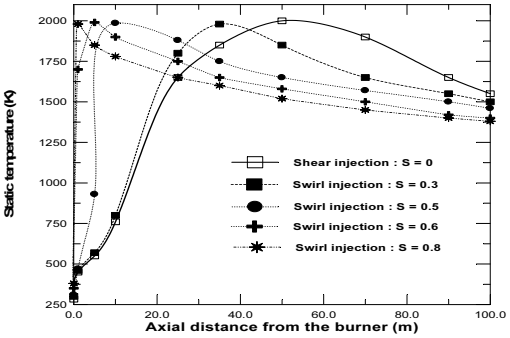

Fig. 11 Static temperature profiles vs. the axial distance for different swirl numbers

Fig. 12 further clarifies the antagonist behavior noticed between the exit *NO* level and the flame-to-burner distance with respect to the injection swirl number (S_0). The reported *NO* emission rate is a mass-weighted averaging over the exit section of the furnace. A compromising solution seems to be possible in the range of moderate swirl numbers ($0.5 \geq S_0 \geq 0.4$). Technologically, this solution would be interesting from both environmental and safety contexts. Indeed, for a swirl number S_0 close to 0.5, the *NO* pollution level exhibits a relative decrease of 28% ($Y_{NO} \leq 1200$ ppm) compared to the original emission rate of the furnace whereas, the flame seems to be relatively distant (about 15 m) from the burner head.

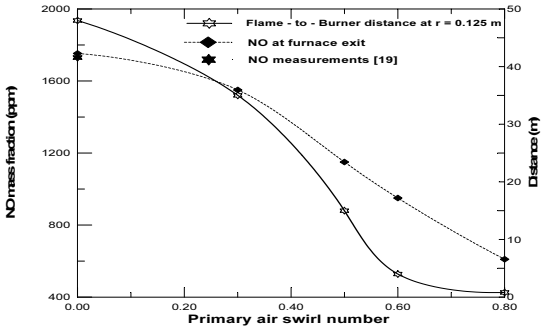

Fig. 12 Effect of swirl on flame - burner distance and exit *NO* emission

4. Conclusion

The main topic of this study has been to carry out a numerical investigation of flow characteristics and *NO* emissions in a full-scale furnace designed for cement production.

To deepen our understanding of the thermal and dynamic fields, as well as emissions of *NO*, the radiative transfer equation has been included in the energy equation using the discrete ordinates model.

In light of the obtained results, we can conclude that the *NO* emission at the furnace exit was found to be sensitive to the inlet conditions. Indeed, co-flow temperature increasing beyond the value 1300 K was in favor of a high production rate of nitrogen oxides. In addition, an attempt towards *NO* depress has been proposed via implementing a swirling configuration for the primary air. Also, through our simulations, we found that a relatively low swirl number ranging from 0.4 to 0.5 allows providing an acceptable *NO* level at the furnace exit. Moreover, this moderate swirl has been shown to keep away the burner head from the flame. It is worth noting that the obtained numerical results are quite similar to experiment results. Nonetheless, further modelling approaches should be addressed in order to better study the unsteadiness of the injection and its impact on both thermal level and *NO* emissions. Improved numerical efficiency of these approaches would accelerate their applications to practical combustion systems.

References

1. **Emad, B.; Gholamreza, Z.; Ezzatollah, S.; Alireza, B.** 2013. Global strategies and potentials to curb CO_2 emissions in cement industry, J. of Cleaner Production 51: 142-161. http://dx.doi.org/10.1016/j.jclepro.2012.10.049.
2. **Bowen, P.** 2011. Combustion hazards posed by hybrid fuel systems, Proc. of the Europ. Combustion Meeting, Cardiff, June 28-July 1, UK.
3. **Streitman, F.L.; Carter, T.B.; Hawkins, G.J.** 1999. Regulation and control of NO_x emissions from the portland cement industry, Proc. of the 92nd Air and Waste Management Meeting, June 20-24, St. Louis, Missouri, USA.
4. **Lin, M.L.; Knenlein, M.J**. 2000. Cement kiln NO_x reduction experience using the NO_x-OUT process, Proc. of the

Joint Power Generation Conference, July 23-26, Miami, Florida, USA.
5. **Caton, J.A.; Xia, Z.** 2004. The selective non catalytic removal (SNCR) of nitric oxides from exhaust streams: comparison of three processes, J. Eng. for Gas Turbines and Power 126(2): 234-240. http://dx.doi.org/10.1115/1.1688366.
6. **Ruifeng, D.; Hongfang, L.; Yunsong, Y.: Zaoxiao, Z.** 2012. A feasible process for simultaneous removal of CO_2, SO_2 and NO_x in the cement industry by NH_3 scrubbing, Applied Energy 97: 85-191.
7. **Young, G.L; von Seebach, M.** 1999. NO_x abatement in kiln plants in the cement industry, Zement-Kalk-Gips 52(6): 304-321.
8. **Possamai, T.S.; Oba, R.; Nicolau, V.P.** 2012. Numerical and experimental thermal analysis of an industrial kiln used for frit production, Applied Thermal Engineering 48: 414-425. http://dx.doi.org/10.1016/j.applthermaleng.2012.05.025
9. **Colannino, J.** 2006. Modelling of Combustion Systems: A Practical Approach, 1st Ed. CRC Press, 680 p.
10. **Launder, B.E.; Spalding, D.B.** 1974. The numerical computation of the turbulent flows, Comp. Methods in Applied Mechanical Engineering 3: 269-289. http://dx.doi.org/10.1016/0045-7825(74)90029-2.
11. **Westbrook, C.K.; Dryer, F.K.** 1981. Simplified reaction mechanisms for the oxidation of hydrocarbon fuels in flames, Combustion Sci. and Technology 27: 31-43. http://dx.doi.org/10.1080/00102208108946970.
12. **Magnussen, B.F.; Hjertager, B.H**. 1976. On Mathematical Models of Turbulent Combustion with Special Emphasis on Soot Formation and Combustion, Int. Symp. on Combustion, 16-20 August, Pittsburg, USA.
13. **Raithby, G.D.; Chui, E.H.** 1990. A finite-volume method for predicting a radiant heat transfer in enclosures with participating media, J. Heat Transfer 112: 415-423. http://dx.doi.org/10.1115/1.2910394.
14. **Hill, S.C.; Douglas, S.L.** 2000. Modelling of nitrogen formation and destruction in combustion systems, Prog. Energy Combust. Sci. 26(5): 417-458. http://dx.doi.org/10.1016/S0360-1285(00)00011-3.
15. **Bowman, C.T.** 1991. Chemistry of Gaseous Pollutant Formation and Destruction, 1st Ed. J. Wiley & Sons, 215 p.
16. **Westenberg, A.A.** 1971. Kinetics of NO and CO in lean premixed hydrocarbon air flames, Combustion Science and Technology 4(1): 59-64. http://dx.doi.org/10.1080/00102207108952472.
17. **Fluent V.6.3.26.** 2006. Fluent Inc, NH, USA.
18. **Sturgess, G.J.; Syed, S.A.; McMaus, K.R**. 1983. Importance of inlet boundary conditions for numerical simulation of combustors flows, AIAA-83-1263.
19. **Nial, M.; Loukarfi, L.; Benarous, A**. 2009. Turbulent flame behaviour in a confined combustor: application to cement furnaces, Proceeding of the French Mechanical Congress (CFM), August 24- 28, Marseille, France.
20. **Benarous, A.; Karmed, D.; Champion, M.; Liazid, A.** 2011. Numerical study of a partially premixed flame using the LW-P model, Proc. of the European Combustion Meeting, June 28 -July 1, Cardiff, UK.
21. **Benarous, A.; Liazid, A.; Loukarfi, L.; Karmed, D.** 2010. CFD investigation on pollutant production in a cement industrial furnace, Proc. of ICAMMM, 13-15 December, Muscat, Sultanate of Oman.
22. **Pope, S.B.** 1978. An explanation of the turbulent round-jet / plane-jet anomaly, AIAA Journal 16(3): 279-281. http://dx.doi.org/10.2514/3.7521.
23. **Lien, F.S.; Leschziner, M.A.** 1994. Assessment of turbulent transport models including non-linear rng eddy-viscosity formulation and second-moment closure, Computers and Fluids 23(8): 983-1004. http://dx.doi.org/10.1016/0045-7930(94)90001-9.
24. **Launder, B.E.; Reece, G.J.; Rodi, W.** 1975. Progress in the development of a reynolds-stress turbulence closure, J. Fluid Mech. 68(3): 537-566. http://dx.doi.org/10.1017/S0022112075001814.

A. Mokhtardidouche, A. Benarous, L. Loukarfi, H. Naji

SKAITMENINĖ NO_x EMISIJOS PROGNOZĖ NATURALAUS DYDŽIO KROSNYJE

R e z i u m ė

Šiame straipsnyje pateikiama šilumos kiekio ir azoto oksidų emisijos greičio nustatymo pramoninėje krosnyje skaitmeninė prognozė. Favre suvidurkintos būvio lygtys, išspinduliuojamos šilumos nuostolių skaičiavimui, išspręstos baigtinių tūrių metodu. Turbulentiniai tekėjimai uždaromi naudojant $k-\varepsilon$ modelį, kuriam pritaikyta Pope pataisa. Aprašant dviejų pakopų cheminės/turbulentinės sąveikos įtaką nesumaišytai liepsnai naudotas Magnussen relaksacijos modelis. Taip pat ištirtas sūkurių skaičiaus poveikis. Prognozuojama statinė temperatūra kaip ir NO emisijos greitis ties krosnies anga sutapo su atliktais matavimais. Be to skaičiavimo rezultatai parodė, kad NO greičio sumažėjimas 28% pasiektas sukūrus nedidelį sūkurį paduodant orą.

A. Mokhtardidouche, A. Benarous, L. Loukarfi, H. Naji

NUMERICAL PREDICTION OF NO_X EMISSIONS IN A FULL-SCALE FURNACE

S u m m a r y

The present paper deals with a numerical prediction of the thermal level and emission rate of nitrogen oxides within an industrial furnace. Favre averaged forms of the governing equations accounting for radiative heat losses are solved via a finite volume formulation. Turbulent fluxes are closed using a $k-\varepsilon$ model for which a limited Pope correction is performed. The relaxation model of Magnussen is used to describe the two-step chemistry/turbulence interaction for the non-premixed flame. The effect of the swirl number has been also investigated. The predicted static temperature as well as *NO* emission rate at the furnace exit show good agreement with in-situ measurements. In addition, the numerical computation shows that the depression is about 28% for the rate of *NO*, which it is obtained by adopting a moderate swirl at the primary-air entrance.

Keywords: Oxides of nitrogen (NO_x), Emission, Turbulent combustion, CFD simulation, Industrial furnace.

Received March 27, 2013
Accepted February 11, 2014